ISPRS Annals of the Photogrammetry, Remote Sensing and Spatial Information Sciences, Volume XI-3-2026
XXV ISPRS Congress 2026 “From Imagery to Understanding”, Commission III, 4–11 July 2026, Toronto, Canada

Effectiveness of Airborne LiDAR Intensity for Identifying Surface Fire Burned Areas in Wildfires

Takafumi Kakuno, Junichi Takanuki, Takaaki Ankai, Takumi Satou

AERO TOYOTA CORPORATION, Japan - (takafumi-kakuno, Junichi- tkanuki, takaaki-ankai, Takumi-satou) @aerotoyota.co.jp

Keywords: LiDAR Intensity analysis, Ground return intensity, Burned area delineation, Wildfire damage assessment, Forest type comparison

Abstract

Wildfires induce significant changes in forest structure and the surface reflectance characteristics. This study evaluated the effectiveness of using airborne LiDAR Intensity data to delineate surface fire burn areas in wildfires. We extracted ground returns from both coniferous and deciduous forests and conducted qualitative assessment of Intensity through Intensity images, as well as statistical evaluation using the non-parametric Mann–Whitney U test to compare burned and unburned areas. We compared the median and standard deviation of Intensity at a 10-m mesh scale, calculating standard deviation at a finer 0.5-m mesh resolution. The results revealed significant differences between burned and unburned areas. The effect size r for the median in deciduous forests ranged from -0.55 to -0.84, while the effect size r for the standard deviation in coniferous forests ranged from -0.38 to -0.47. Both indicated a medium to large effect. These findings suggest that LiDAR Intensity can effectively identify surface fire burn areas even under heterogeneous forest floor conditions. The proposed method has the potential to contribute to enhancing post-fire monitoring using airborne LiDAR.

1. INTRODUCTION

In Japan, dry conditions between January and April increase the risk of wildfires. Most wildfires originate from human factors such as campfires or controlled burns. Depending on the combustion type, wildfires can be classified as surface fires and crown fires (Van Wagner, 1977). Among these, crown fires are clearly visible from the air, allowing wide use of satellite imagery and aerial photographs to delineate burn areas. While surface fires, which represent the initial stage of wildfire spread, are often obscured by tree trunks and canopies.
Therefore, the specific methodology making accurate aerial identification of burn areas has not been sufficiently established.

Wildfires seriously affect not only forest resources but also ecosystems, soil erosion, regional economies, and public health and safety. Accurate and rapid assessment of damage is essential for post-fire forest management and restoration. Such assessments must also consider increased soil erosion, flood risks, and impacts on wildlife habitats. Climate change has heightened wildfire risks, and recent studies both in Japan and internationally report an increasing frequency and scale of wildfires.

Remote sensing techniques such as optical satellites, SAR, aerial photographs, and airborne LiDAR have been applied to delineate wildfire burn areas. In Japan, researchers have estimated burn areas using the thermal infrared band of Himawari-8 (Mizutani et al., 2017) and evaluated post-fire burn severity using optical and airborne LiDAR data (Gale et al., 2022). Optical satellites provide wide coverage; however, their spatial resolution in visible and infrared bands is typically several tens of meters, limiting direct observation under forest canopies.

SAR-based studies have demonstrated burn area detection through multi-temporal comparisons using Sentinel-1 C-band and ALOS-2 L-band data (Sudiana et al., 2025), as well as change detection before and after wildfires using Sentinel-1 VV/VH polarizations (Hosseini et al., 2023). SAR offers the advantage of cloud- and smoke-penetrating wide-area observations. However, its penetration depth in coniferous sub-canopy-layer is limited for X- and Ku-band sensors (Montomoli et al., 2018), and the method depends on pre-fire data acquisition and revisit cycles, which reduces its timeliness.

An example of burn extent identification using aerial photographs is the two-stage pipeline for burn severity mapping based on unsupervised learning from aerial and satellite imagery (Bai et al., 2024). While 2D imagery alone provides limited information beneath the canopy, combining it with 3D data such as LiDAR can complement these gaps. Moreover, integrating drone-mounted multispectral cameras with 3D point clouds allows quantification of sub-canopy-layer burn by analyzing NDVI changes (Batchelor et al., 2025). This method can assess damage under the canopy that 2D imagery cannot capture. However, point cloud generation is sensitive to light and wind conditions and is limited to localized areas, so combining it with other approaches is recommended for large-scale wildfires.

Examples of Airborne LiDAR applications include post-fire tree condition assessment using canopy and ground models derived from the height information of LiDAR point cloud data (Wing et al., 2010), calculation of existing biomass and pre- and post-fire comparisons using a combination of LiDAR reflectance and Landsat OLI reflectance bands (García et al., 2017), and mapping post-fire habitat characteristics by integrating Landsat and airborne LiDAR data (Vogeler et al., 2016).

Despite these advances in combining 2D and 3D remote sensing data, studies using airborne LiDAR to delineate burn areas of surface fires—the initial phase of wildfire spread—remain limited.

In Japan, local governments primarily conduct burn area assessments on identifying the extent of damage for rapid post-fire recovery and restoration. Conventional aerial photography of the situation is conducted multiple times from the time a fire breaks out until it is extinguished, but these surveys typically offer only rough estimates. Detailed post-fire investigations rely on field surveys, which present logistical and cost challenges. Consequently, remote sensing techniques capable of providing detailed burn area delineation are highly anticipated.

Between January and March 2025, several wildfires occurred in Japan. According to the Forestry Agency, the total burned area during this period reached approximately 5,000 ha, significantly exceeding the five-year average annual burned area of roughly 700 ha. Notably, a wildfire in February in Ōfunato City, Iwate Prefecture, represented an unusually large-scale event (Figure 1). Ōfunato’s forests cover 26,132 ha, about 81% of the city’s area. The fire destroyed approximately 3,370 ha, equivalent to about 12% of the forest area, and damaged 226 buildings. Local surveys estimated the economic loss at 2.9 billion JPY.

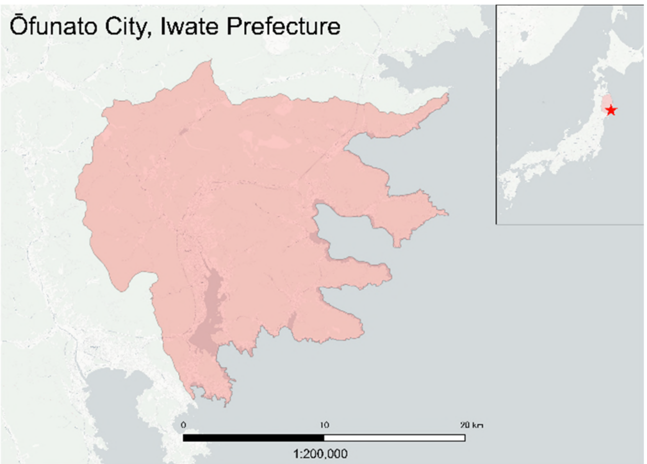

Figure 1. Location of the study area in Japan and within Iwate Prefecture. The red polygon indicates Ofunato City. Basemap data © CARTO.

This study focuses on early assessment of the burn area in this wildfire using airborne LiDAR point cloud Intensity data. LiDAR Intensity varies depending on the material, color, and surface characteristics of illuminated objects. After a wildfire, combustion alters the surface properties, resulting in changes in surface reflectance. Such changes can potentially be captured by LiDAR Intensity. This study evaluates the effectiveness of delineating surface fire burn areas using airborne LiDAR Intensity.

The novelty of this study lies in using LiDAR Intensity to overcome limitations of existing methods, such as the absence of pre-fire data and difficulty in aerial visual observation. Immediate analysis of acquired data enables rapid and accurate burn area identification, supporting efficient information acquisition during initial disaster response. Furthermore, statistical analysis demonstrates that relative differences in LiDAR Intensity can serve as empirical indicators for delineating surface fire burn areas.

2. Data and Methods

2.1 Study Area and Data Specification

This study used airborne LiDAR point cloud data to assess the burned area of a wildfire that occurred in Ōfunato City, Iwate Prefecture, Japan, in 2025 (Figure 2). The boundary of the burned area shown in the Figure 2 was traced and delineated from the official report published by the Fire and Disaster Management Agency (Fire and Disaster Management Agency, 2025).

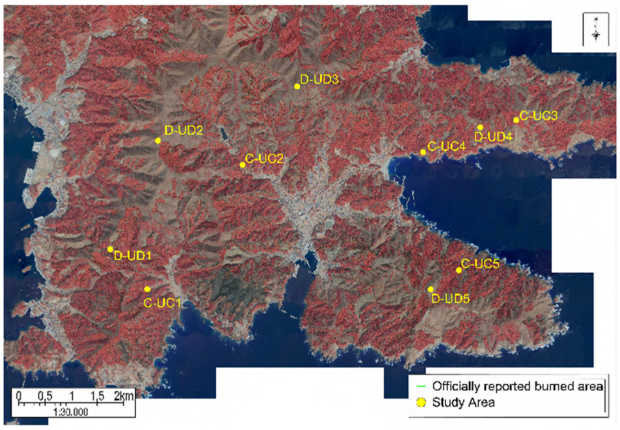

Figure 2.Overview of study area overlaid on CIR imagery.

The LiDAR data were acquired using a Leica Geosystems TerrainMapper2, operating at a wavelength of 1064 nm. The point density of the acquired LiDAR data was approximately 10 points/m². The point cloud included 3D coordinates and Intensity information. Since burned and unburned areas were comprehensively captured under identical acquisition conditions, Intensity values were not normalized and were used directly as relative comparison indicators reflecting the measurement and environmental conditions.

In this study, the LiDAR point cloud data used is compared and evaluated using the following two patterns:

1. All returns: all acquired point clouds
2. Ground returns: point clouds limited to areas affected by surface fire

To obtain Ground returns, we first classified the point cloud into ground points using point cloud editing software. We then extracted sample data to compare statistical differences between burned and unburned areas. Using burn assessment results based on Intensity images, we selected burned and unburned areas for coniferous and deciduous forests at a 10-m mesh scale. The analysis covers a total of 20 extracted meshes, including 5 points each from the burned area (C) and unburned area (UC) in coniferous forests, and 5 points each from the burned area (D) and unburned area (UD) in deciduous forests (Figure 3). The mesh size was set to 10 m based on the consideration that laser light passing through coniferous forest trunks would result in fewer ground return points. The total number of points in All returns used for analysis was 75,197, of which 18,994 points (approximately 25%) were Ground returns (Table 1).
Ground classification was conducted using standard filtering algorithms implemented in commercial point cloud processing software, which separate ground points based on elevation continuity and local slope criteria. Isolated points and extreme Intensity outliers caused by sensor noise or multi-path effects were excluded prior to statistical analysis. Meshes with extremely low ground point density were retained only when a minimum number of ground returns was satisfied to ensure statistical robustness.

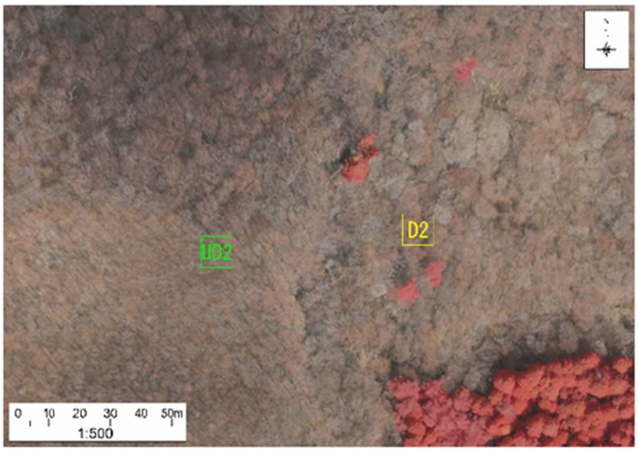

Figure 3. Overview of the study areas and the representative site overlaid on CIR imagery.

	file	All returns Number of points	Ground returns Number of points	Percentage (%)
Burned Coniferous forests	C1	2450	159	6.5
	C2	2599	145	5.6
	C3	2792	204	7.3
	C4	2625	217	8.3
	C5	3220	253	7.9
Burned Deciduous forests	D1	2469	1078	43.7
	D2	7356	1918	26.1
	D3	3658	1245	34.0
	D4	4712	1587	33.7
	D5	5962	1874	31.4
Unburned Coniferous forests	UC1	2608	270	10.4
	UC2	3707	593	16.0
	UC3	2782	354	12.7
	UC4	3654	609	16.7
	UC5	2764	436	15.8
Unburned Deciduous forests	UD1	2668	1096	41.1
	UD2	6975	2034	29.2
	UD3	3536	1326	37.5
	UD4	4038	1706	42.2
	UD5	4622	1890	40.9
Total		75197	18994	25.3

Table 1. Summary of LiDAR point counts for each analysis area.

2.2 Ground Truth Data

Ground truth data were collected through limited field surveys to confirm whether selected sample areas were burned or unburned. Based on the burn damage assessment using LiDAR Intensity imagery, representative locations within coniferous forest (C1–UC1) and deciduous forest (D2–UD2) were visited to verify surface conditions such as charring, ash deposition, and the presence or absence of residual vegetation (Figure 4).

It should be noted that the ground surveys were not intended to precisely delineate burn boundaries in the field. Instead, they served as qualitative validation to confirm the burn status of sample meshes used in the statistical analysis. The primary delineation of burned areas relied on airborne LiDAR Intensity data, while the official burn perimeter reported by the Fire and Disaster Management Agency (Fire and Disaster Management Agency, 2025) was used only as a reference for the overall fire extent.

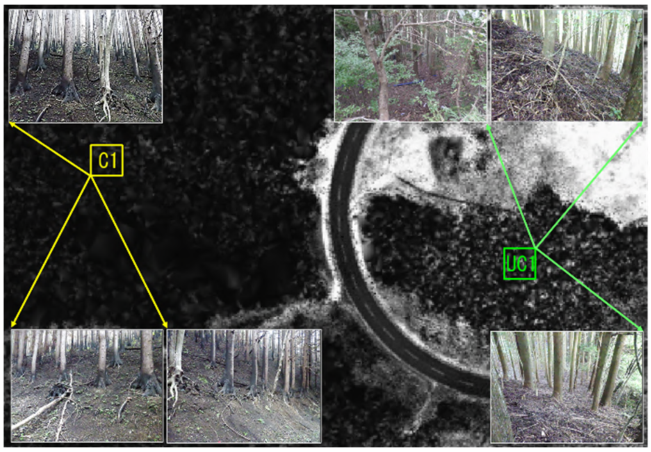

Figure 4. Field photograph of site C1-UC1.

2.3 LiDAR Intensity Image Generation and Visual Assessment

To visualize surface fire burn areas, we generated rasterized Intensity images from the All returns and Ground returns. Based on the point density of 10 points/m², we set the raster resolution to 0.5 m. Intensity values were interpolated using the Triangulated Irregular Network (TIN) method, and the mean value of points within each raster cell was assigned. We qualitatively evaluated burn area visibility by comparing the Intensity images generated from All returns and Ground returns (Figure 5).

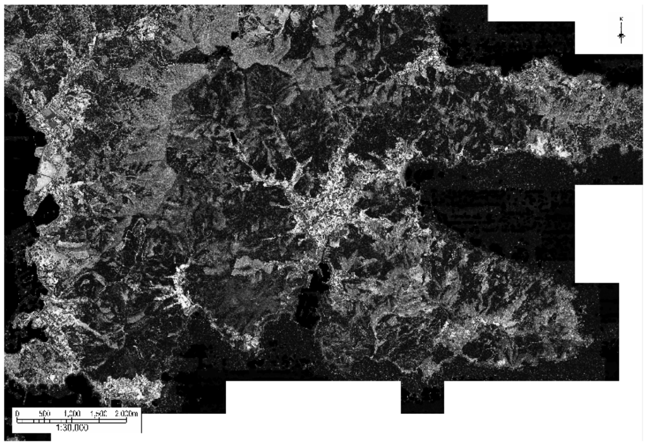

Figure 5. Intensity imagery of Ground-returns.

2.4 Quantitative Analysis at 10 m Mesh Level

For the 20 selected meshes, we calculated the mean, median, and standard deviation (STD) of Intensity for both All returns and Ground returns. We created scatter plots using the median and standard deviation values to quantitatively assess the effectiveness of Ground returns in identifying surface fire burn areas.

2.5 Statistical Evaluation

We evaluated the statistical differences in Intensity between burned and unburned areas for Ground returns in both coniferous and deciduous forests. Because LiDAR Intensity distributions can be non-normal and heteroscedastic, we applied the non-parametric Mann–Whitney U test (Mann and Whitney, 1947) to compare the median and STD of Intensity between the two groups.

For evaluating STD, we further subdivided each 10-m mesh into 0.5-m sub-meshes and calculated the STD in each sub-mesh before performing statistical analysis. The U statistic was computed using the ranks of Intensity values, and the smaller of $U1$ and $U2$ was used. U was then converted to a standardized Z value using the following formula:

$$Z = \frac{U - \frac{n_1 n_2}{2}}{\sqrt{\frac{n_1 n_2 (n_1 + n_2 + 1)}{12}}} \quad (1)$$

The p-value corresponding to a two-tailed test is calculated using the following formula:

$$p = 2 \cdot \phi(-|Z|) \quad (2)$$

Statistical significance was determined at this significance level $p < 0.05$. In addition to the Mann–Whitney U test, the effect size r was calculated based on the following to quantitatively indicate the substantive magnitude of the difference between the two groups. Effect sizes were calculated according to the method described by Cohen (1988):

$$r = |Z| / \sqrt{N} \quad (3)$$

Effect sizes of 0.1, 0.3, and 0.5 correspond to small, medium, and large effects, respectively. The sign of r reflects the relative magnitude of medians between the two groups. Denoting the medians of burned and unburned groups as X_{burned} and $X_{unburned}$, the sign of r was defined as follows:

$$sign(r) = \begin{cases} +1 (X_{burned} > X_{unburned}) \\ -1 (X_{burned} < X_{unburned}) \end{cases} \quad (4)$$

Positive r indicates that the burned group tends to have higher Intensity than the unburned group, whereas negative r indicates the opposite.

The statistical differences in Intensity were summarized using tables and box plots. In the box plots, the box represents the interquartile range (IQR) from the first quartile (Q1) to the third quartile (Q3), visually illustrating the spread around the median. Additionally, values exceeding 1.5 times the interquartile range (IQR) and falling below the first quartile (Q1) or above the third quartile (Q3) are designated as outliers.

3. RESULTS

3.1 Visual Assessment of Burned Areas

In coniferous forests, All returns included high Intensity values from tree canopies, which increased overall Intensity and masked surface-level changes caused by wildfire. As a result, differences between burned and unburned areas were visually ambiguous in the Intensity images, making surface fire delineation difficult.

Similarly, in deciduous forests, Intensity images generated from All returns appeared as uniformly dark surfaces with limited contrast. This reflects the dominance of canopy-level returns, which obscures surface reflectance differences associated with fire damage. These results indicate that visual interpretation based solely on All returns is insufficient for identifying surface fire burn areas.

In contrast, Ground returns effectively isolated surface-level information, enabling clearer visualization of Intensity differences related to burning. This highlights the importance of return selection prior to quantitative analysis. (Figure 6).
In coniferous forests, unburned areas displayed a mixture of high-Intensity white cells and low-Intensity black cells, whereas burned areas showed a uniform distribution of black cells. Additionally, the Intensity images exhibited a characteristic pattern in which this uniform darkening in burned zones made the boundaries of the burned extent visually distinguishable. (Figure 7).

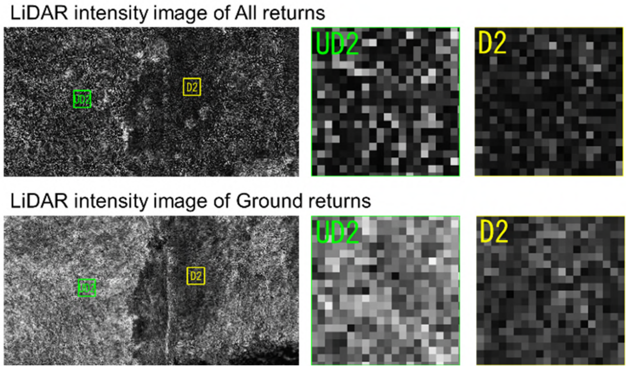

Figure 6. Visualization of LiDAR intensity for All returns and Ground returns in Deciduous forests.

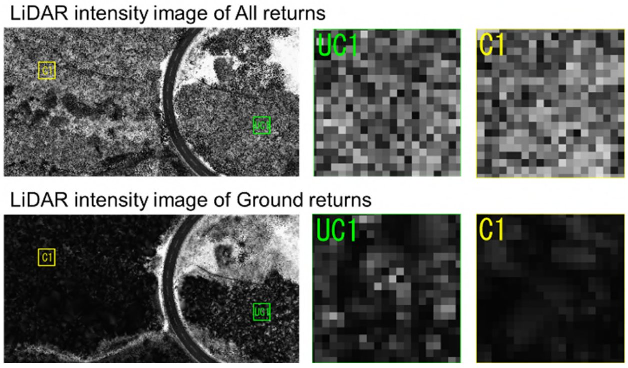

Figure 7. Visualization of LiDAR intensity for All returns and Ground returns in Coniferous forests.

3.2 Quantitative Characteristics of Burned and Unburned Areas

We created scatter plots of Intensity using the median and STD for both All returns and Ground returns. The following characteristics were observed:
In deciduous forests for All returns (Figure 8), unburned areas exhibited a large STD of approximately 300–500, whereas the median Intensity showed no significant difference between burned and unburned areas. Overall, the Intensity remained very low, below 200. In coniferous forests, both median and STD of burned and unburned areas showed similar distributions, and no clear differences emerged.

For Ground returns (Figure 9), deciduous forests exhibited a clear difference in median Intensity between burned and unburned areas. Burned areas had median Intensity below 400, whereas all unburned samples exceeded 600. The difference reached approximately 200 Intensity units. In coniferous forests, median Intensity showed no notable difference between burned and unburned areas, but burned areas displayed a very low STD concentrated around 100. In contrast, unburned areas exhibited broader variability, with Intensity values above 200 showing substantial spread.

Although median Intensity values in coniferous forests showed limited separation between burned and unburned areas, the standard deviation (STD) revealed distinct differences. This indicates that variability-based metrics are more sensitive to surface fire effects in forests with limited ground penetration, motivating the use of STD as a primary indicator in subsequent statistical analyses.

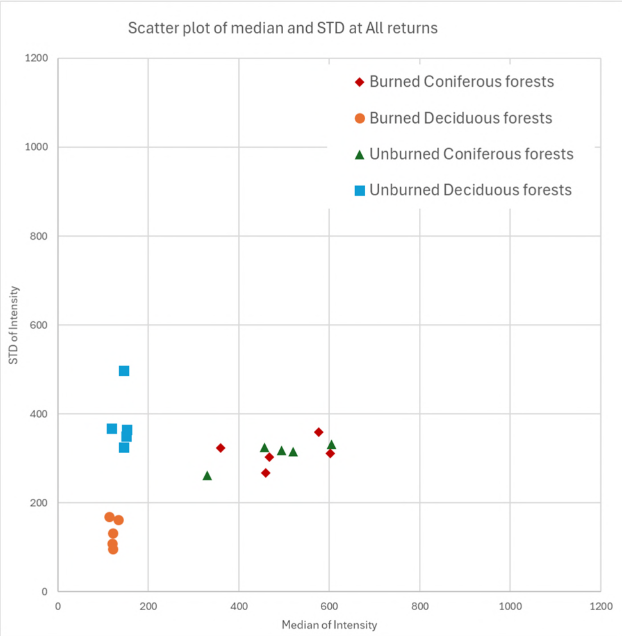

Figure 8. Scatter plot of Median and STD intensity at All returns.

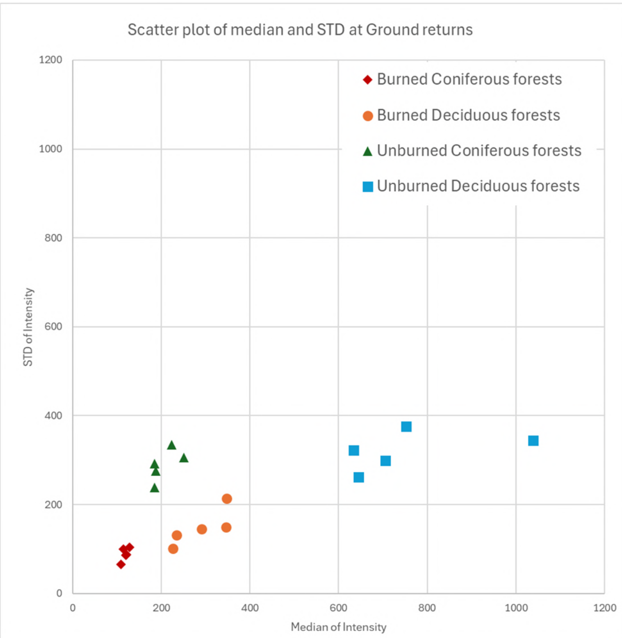

Figure 9. Scatter plot of Median and STD intensity at Ground returns.

3.3 Statistical Evaluation Using Mann–Whitney U Test

We conducted statistical evaluations of median and STD using the Mann–Whitney U test for Ground returns, focusing on characteristics observed in the scatter plots. Based on the observed trends, we analyzed the median for deciduous forests and the STD for coniferous forests.

Figure 10 and Table 2 present the results of the Mann–Whitney U test on median Intensity. In deciduous forests, the Box plot of burned areas appeared lower than that of unburned areas, with a narrow IQR, indicating low variability and uniformly low Intensity. Minimal overlap occurred between burned and unburned Box plots, and the effect size r ranged from -0.55 to -0.84, indicating a very large effect. In contrast, in coniferous forests, although extremely low reflectance values were observed within the burned areas, the box plots for burned and unburned areas overlapped. The effect size r, expressed quantitatively, ranged from -0.22 to -0.39, indicating a limited effect compared to the results from deciduous forests.

Group	n_burned	n_unburned	U	p	Z	r	r interpretation
C1	159	270	15886.50	6.88E-06	-4.498	-0.217	small
C2	145	593	18648.00	3.72E-26	-10.579	-0.389	medium
C3	204	354	24446.00	2.04E-10	-6.358	-0.269	small
C4	217	609	40252.50	1.16E-17	-8.557	-0.298	small
C5	253	436	36448.50	1.11E-13	-7.427	-0.283	small
D1	1078	1096	177668.00	2.67E-175	-28.228	-0.605	large
D2	1918	2034	720018.50	3.07E-258	-34.327	-0.546	large
D3	1245	1326	20404.00	<1e-308	-42.797	-0.844	large
D4	1587	1706	288608.00	<1e-308	-39.070	-0.681	large
D5	1874	1890	315572.50	<1e-308	-43.658	-0.712	large

Table 2. Table of Mann-Whitney U Test Results for Median Intensity of Ground returns.

Next, the results of the statistical evaluation based on the standard deviation shown in Figure 11 and Table 3 are summarized below. In coniferous forests, the IQR of the burn extent was small, and the reflectance values were consistently concentrated at low levels, indicating that the variability in reflectance was extremely low. In unburned areas, the wider IQR suggested greater variability in Intensity. Based on these patterns, the effect sizes for STD ranged from -0.38 to -0.47, showing moderate effects. In coniferous forests, STD provided higher sensitivity for detecting burn areas than the median.
Overall, the results confirmed visually and quantitatively that burned areas in Wildfires exhibited generally low Intensity and reduced variability in STD. Furthermore, the Mann–Whitney U test and effect size analyses demonstrated that Wildfires caused statistically significant changes in ground surface Intensity. These findings suggest that LiDAR Intensity can serve as an effective indicator for identifying burned areas and assessing fire impact.

Group	n_burned	n_unburned	U	p	Z	r	r interpretation
C1	29	62	375.00	8.24E-06	-4.463	-0.468	medium
C2	20	181	308.50	1.20E-09	-6.083	-0.429	medium
C3	37	84	676.50	8.07E-07	-4.936	-0.449	medium
C4	37	183	1471.50	6.00E-08	-5.420	-0.365	medium
C5	56	115	1731.00	9.61E-07	-4.901	-0.375	medium
D1	343	356	38174.50	1.01E-17	-8.573	-0.324	medium
D2	397	422	33608.00	1.02E-49	-14.825	-0.518	large
D3	372	373	12980.50	3.55E-82	-19.202	-0.704	large
D4	389	395	13786.00	5.59E-88	-19.884	-0.710	large
D5	394	403	28617.50	4.92E-55	-15.625	-0.553	large

Table 3. Table of Mann-Whitney U Test Results for STD Intensity of Ground returns.

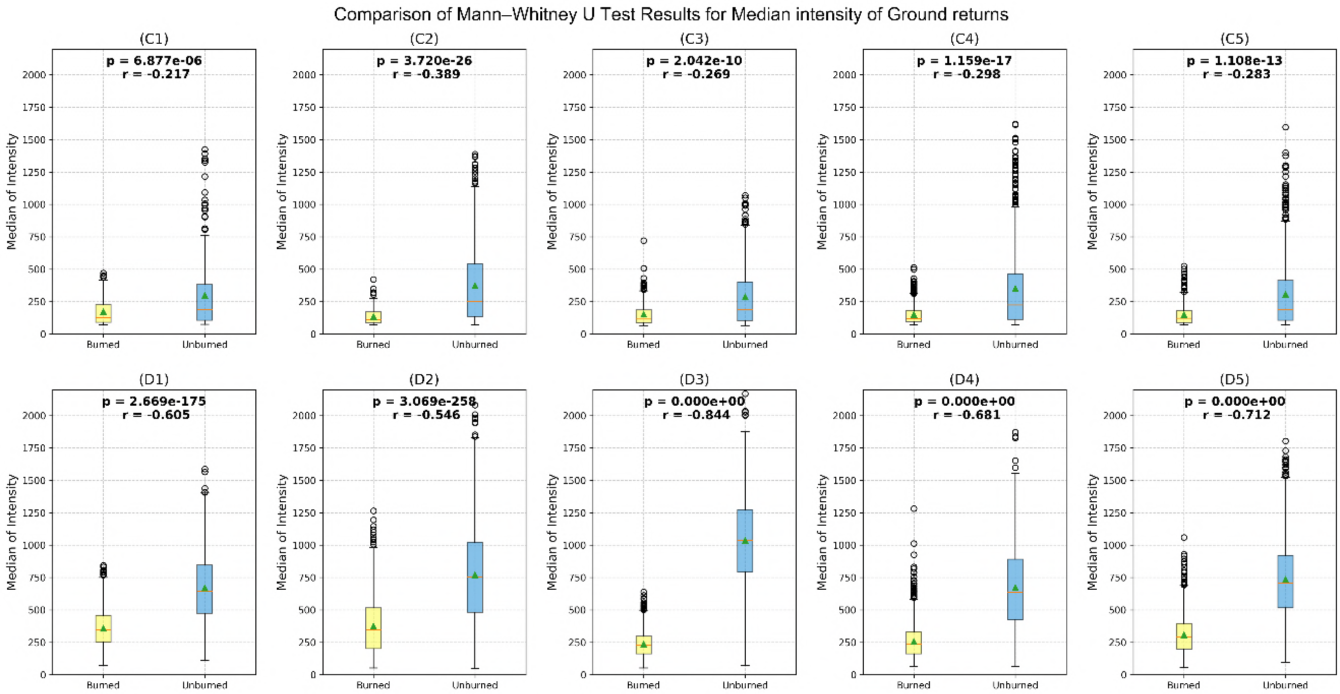

Figure 10. Comparison of Mann-Whitney U Test Results for Median Intensity of Ground returns.

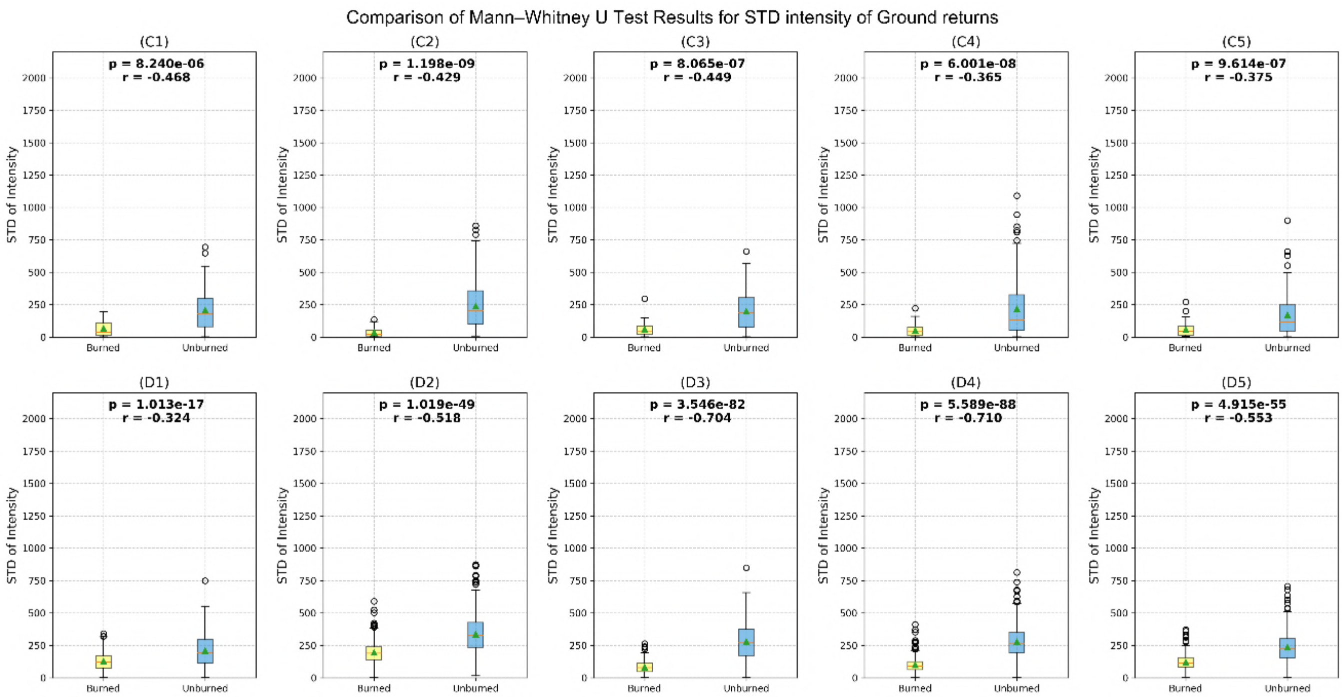

Figure 11. Comparison of Mann-Whitney U Test Results for STD Intensity of Ground returns.

4. DISCUSSION

The observed decrease in LiDAR Intensity within burned areas is consistent with previous studies reporting reduced reflectance due to vegetation loss, charring, and exposure of mineral soil following fire events (Wing et al., 2010; Vogeler et al., 2016). Similar reductions in surface reflectance have been widely reported using optical indices such as the Normalized Burn Ratio (NBR), although optical sensors are limited in their ability to capture sub-canopy fire effects (Gale et al., 2022).

Compared to optical and SAR-based approaches, LiDAR Intensity provides unique advantages in resolving surface fire impacts beneath forest canopies, particularly when ground returns are selectively analyzed.

Statistical comparisons showed that the median Intensity of burned areas was significantly lower than that of unburned areas in both forest types, demonstrating a clear reduction in surface reflectance following fire events. The effect size r ranged from -0.22 to -0.39 in coniferous forests, indicating a small effect, and from -0.55 to -0.84 in deciduous forests, indicating a large effect. These results suggest that the reduction in Intensity reflects the loss of vegetation and litter layers, as well as the charring or exposure of mineral soil caused by burning. In deciduous forests, abundant surface fuels promote the spread of surface fires, leading to pronounced darkening and carbonization of the ground surface, which results in a stronger decrease in Intensity.

Furthermore, all analyzed meshes exhibited significant differences in STD between burned and unburned areas. The effect size r ranged from −0.38 to −0.47 in coniferous forests, indicating a moderate effect, and from −0.32 to −0.71 in deciduous forests, indicating a relatively large effect. In unburned areas, residual understory vegetation and partially exposed soil produced spatial heterogeneity in surface reflectance. Conversely, in burned areas, the removal of vegetation and the formation of a homogenized, carbonized surface reduced spatial variability in reflectance, as represented by lower STD values (Figure 12).

However, several limitations remain in this study. The LiDAR system used employed a near-infrared wavelength of 1064 nm, which is easily absorbed by moist surfaces or water-rich materials. Therefore, immediately after firefighting or rainfall events, wet surfaces may exhibit artificially low Intensity values, potentially reducing the accuracy of surface fire burn area detection.

The collection of Ground truth data also presents challenges. In the target area of Ōfunato City, Iwate Prefecture, the total forest area is 26,132 ha, consisting of 1,776 ha of national forest and 24,356 ha of private forest. The private forest area includes 16,971 ha under private ownership, 5,023 ha under municipal ownership, and 2,362 ha under prefectural ownership (Fire and Disaster Management Agency, 2025). Obtaining Ground truth data requires access permission from landowners. In large-scale wildfire events such as the one in Ōfunato, private landownership constraints often limit field access, resulting in insufficient Ground truth coverage.

The limitations of this study can be summarized as follows. The LiDAR system used in this study operates at a wavelength of 1064 nm in the near-infrared region, which is known to be readily absorbed by moist surfaces and objects with high water content. As a result, reflectance intensity may be underestimated under wet surface conditions, such as immediately after fire suppression activities or following rainfall, potentially affecting the accurate delineation of surface fire burn areas. Furthermore, because Intensity values were not radiometrically calibrated, transferability to other sensors or acquisition conditions should be examined in future studies.

In addition, physical occlusion of laser beams by forest canopies remains a significant constraint. As shown in Table **1** the proportion of ground returns in coniferous forests is limited to approximately 5–15%, leading to a reduced ground penetration rate. Consequently, in evergreen broadleaf forests with dense canopies, even during the leaf-off season, laser beams are less likely to reach the ground surface compared to coniferous forests. This limitation hampers reliable characterization of ground surface conditions and may further reduce the accuracy of surface fire burn area delineation.

These findings emphasize the importance of return selection and forest structure consideration when using LiDAR Intensity for post-fire assessments. Future studies should aim to improve burn area detection accuracy across diverse forest environments by integrating multi-wavelength LiDAR systems and complementary datasets such as hyperspectral imagery.

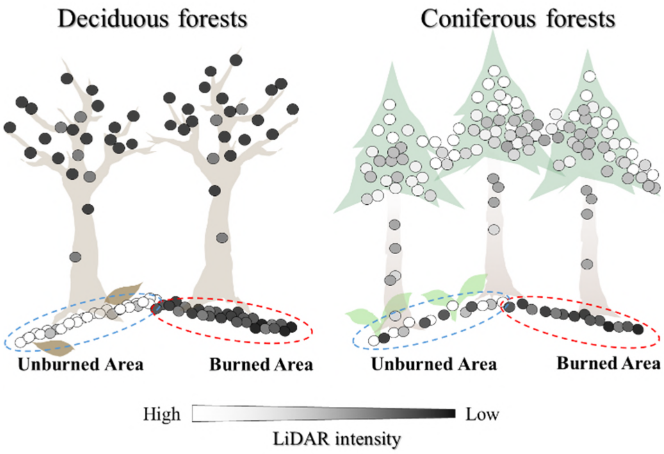

Figure 12. Schematic illustration of surface fire burned area detection using LiDAR intensity.

5. CONCLUSIONS

This study demonstrated the effectiveness of airborne LiDAR Intensity for delineating surface fire burn areas in Japanese forests. Significant differences in median Intensity were observed in deciduous forests, while standard deviation provided higher sensitivity in coniferous forests where ground returns were limited.

The results indicate that LiDAR Intensity enables high-resolution identification of surface fire impacts without relying on pre-fire data, supporting rapid post-disaster assessment. Although sensor- and condition-dependent limitations remain, this approach shows strong potential for enhancing wildfire damage assessment and forest management practices.

ACKNOWLEDGMENTS

The authors would like to express their sincere appreciation to the disaster response agencies for providing valuable insights toward the practical and social implementation of this technology.

The authors also wish to extend their heartfelt sympathies to all those affected by the disaster.

REFERENCES

Bai, T., Ge, L., Sepasgozar, S. M. E., Sheng, Z., Liu, C., Wu, Y., Zhang, Q. 2024. Unsupervised bushfire burn severity mapping using aerial imagery and point clouds. *ISPRS Annals of the Photogrammetry, Remote Sensing and Spatial Information Sciences*, X-4, 29–36.
https://doi.org/10.5194/isprs-annals-X-4-2024-29-2024

Batchelor, J. L., Cary, G. J., Yebra, M., Leavesley, A. J., & van Dijk, A. I. J. M. 2025. Drone-based, multispectral photogrammetric point clouds to classify fire severity at differing canopy height strata. *Fire Ecology*, 21(1), 45–63. https://doi.org/10.1186/s42408-025-00375-2

Cohen, J., 1988. *Statistical Power Analysis for the Behavioral Sciences*, 2nd ed. Lawrence Erlbaum Associates, Hillsdale, New Jersey.

Fire and Disaster Management Agency, Ministry of Internal Affairs and Communications, Japan. 2025. Fire Cause Investigation Report on the Forest Fire in Ōfunato City, Iwate Prefecture, February 26, 2025. Tokyo, Japan. (in Japanese)
and Remote Sensing, **56**(5), 244–251. https://www.jstage.jst.go.jp/article/jsprs/56/5/56_244/_pdf/-char/ja

Montomoli, F., et al. 2018. Forest canopy penetration of X-band SAR: A study based on TerraSAR-X data. *Remote Sensing of Environment*, 204, 1–12.
https://doi.org/10.1016/j.rse.2017.10.017

Sudiana, D., Lestari, A. I., Rizkinia, M., Riyanto, I., Vetrita, Y., Bayanuddin, A. A., Putri, F. A., Kartika, T., Suhadha, A. G., Julzarika, A., Sobue, S., Prabuwono, A. S., & Sri Sumantyo, J. T. 2025. Assessing Burned Area Detection in Indonesia Using the Stacking Ensemble Neural Network (SENN): A Comparative Analysis of C- and L-Band Performance. *Computers*, 14(8), Article 337. https://doi.org/10.3390/computers14080337

Van Wagner, C.E., 1977. Conditions for the start and spread of crown fire. Canadian Journal of Forest Research, 7(1), 23–34. https://doi.org/10.1139/x77-004

Vogeler, J. C., Yang, Z., Cohen, W. B. 2016. Mapping post-fire habitat characteristics through the fusion of remote sensing tools. *Remote Sensing of Environment*, 173, 294–303.
https://doi.org/10.1016/j.rse.2015.08.011

Wing, M.G., Eklund, A. & Sessions, J. 2010. Applying LiDAR technology for tree measurements in burned landscapes. *International Journal of Wildland Fire*, 19(1), 104–114.
https://doi.org/10.1071/WF081

https://www.soumu.go.jp/main_content/001026714.pdf

Gale, M. G., Cary, G. J., Yebra, M., Leavesley, A. J., & van Dijk, A. I. J. M. 2022. Comparison of contrasting optical and LiDAR fire severity remote sensing methods in a heterogeneous forested landscape in south-eastern Australia. *International Journal of Remote Sensing*, 43(7), 2538–2559.
https://doi.org/10.1071/WF21131

García, M., Saatchi, S., Casas, A., Koltunov, A., Ustin, S., Ramirez, C., Garcia-Gutierrez, J., & Balzter, H. 2017. Quantifying biomass consumption and carbon release from the California Rim fire by integrating airborne LiDAR and Landsat OLI data. *Journal of Geophysical Research: Biogeosciences*, 122(2), 340–353.
https://doi.org/10.1002/2015JG003315

Hosseini, M., and Lim, H.S., 2023. Burned area detection using Sentinel-1 SAR data: A case study of Kangaroo Island, South Australia. *Applied Geography*, 151, 102854. https://doi.org/10.1016/j.apgeog.2023.102854

Mann, H.B., and Whitney, D.R., 1947. *On a Test of Whether One of Two Random Variables is Stochastically Larger than the Other*.
Annals of Mathematical Statistics, 18(1), pp.50–60.
https://doi.org/10.1214/aoms/1177730491

Mizutani, M., Takeuchi, W., & Moriyama, M. 2017. Forest fire detection and burned area estimation using Himawari-8 satellite data in Japan. *Journal of the Japan Society of Photogrammetry*